

Supplementary material for: **Water-compression gating of nanopore transport**

James Wilson[†] and Aleksei Aksimentiev^{*,†,‡}

†Department of Physics, University of Illinois at Urbana–Champaign, 1110 West Green Street, Urbana, Illinois 61801

‡Beckman Institute for Advanced Science and Technology

E-mail: aksiment@illinois.edu

Table of Contents:

Supplementary Methods	S3–7
Sup. Fig. S1: MD simulations of dsDNA capture by graphene nanopore	S8
Sup. Figs. S2 and S3: MD simulations of a 5bp DNA fragment’s capture	S9–10
Sup. Fig. S4: Effect of membrane thickness on the effective force on DNA	S11
Sup. Fig. S5: Effect of ion concentration on the effective force on DNA	S12
Sup. Fig. S6: Effect of pore diameter on the effective force on DNA	S13
Sup. Fig. S7: Effect of restraints strength on the effective force on DNA	S14
Sup. Fig. S8: Effect of simulation cell size on the effective force on DNA	S15
Sup Fig. S9: Effect of transmembrane bias on the maximum electric field strength	S16
Sup. Fig. S10: Effect of transmembrane bias on the average z-component of a water molecule’s dipole moment within a graphene nanopore	S17
Sup. Fig. S11: Effect of transmembrane bias on the maximum dielectrophoretic force .	S18
Sup. Fig. S12: Simulated dependence of solution density on solution pressure	S19
Sup. Fig. S13: Potential of mean force for unphosphorylated villin headpiece	S20
Supplementary Note 1: Effect of access resistance	S21–23
Supplementary Note 2: Finite element calculations	S24–26
Captions to Supplementary Movies 1–4	S27–S30
Supplementary References	S31–32

Supplementary Methods

General MD methods. MD simulations were performed using NAMD,¹ a 2 fs integration time step and hexagonal prism periodic boundary conditions. The CHARMM36 force field² was used to describe DNA, water and ions. Carbon atoms of graphene were modeled as type CA atoms;^{2,3} custom NBFIX corrections were used to describe ion–ion and ion–DNA interactions.⁴ SETTLE⁵ and RATTLE⁶ algorithms were used to describe covalent bonds involving hydrogen in water and DNA molecules, respectively. Van der Waals interactions were evaluated using a smooth 7–8 Å cutoff. Particle mesh Ewald summation⁷ was used to evaluate long-range electrostatic interactions over a 0.1 nm-spaced grid; the full electrostatics calculations were performed every three time steps. A Lowe-Anderson thermostat⁸ maintained the temperature at 295 K with an interaction radius of 2.7 Å and a collision rate of 50 ps⁻¹.

Atomic models of graphene systems. Atomic models of one-, two-, three- and five-layer graphene membranes were generated using VMD’s⁹ Inorganic Builder plugin.¹⁰ Each graphene membrane patch was a hexagon 5.67 nm on side, aligned with the $x - y$ plane of our coordinate system; the geometrical center of each graphene patch was located at the origin. Circular nanopores were created by removing atoms that satisfied the condition $x^2 + y^2 < R^2$, where x and y denote the coordinates of the atoms and R is the target radius of the nanopore; nanopores of radius 14.5, 17.5, and 24.5 Å were created. Water was added using the solvate plugin in VMD, creating a hexagonal prism of 49 Å inner radius and 130 Å height. A 16 basepair fragment of DNA, poly(AT)₈, was generated using the 3D-DART webserver¹¹ and placed coaxial with the nanopore. Potassium and chloride ions were added to neutralize the system and bring the concentration to 1 M using the Autoionize plugin in VMD. Open pore systems (with no DNA present) were built following the same protocol. Each system contained approximately 110,000 atoms.

The atomic coordinates of a villin headpiece protein was obtained from the protein data

bank (PDB ID 2F4K). The protein was placed with its center of mass located at the symmetry axis of the nanopore. The following three phosphorylation states of the protein were modeled: unmodified protein with no phosphorylation, singly phosphorylated variant produced by applying an SP2 patch to serine residue 56 (state P1), and doubly phosphorylated variant produced by applying the SP2 patch to serine residues 56 and 43 (state P2). The net charge of the unphosphorylated variant was that of one proton. The net charge of the villin headpiece in states P1 and P2 was one and three electron charges, respectively. Potassium and chloride ions were added to neutralize the system and bring the concentration to 1 M using the Autoionize plugin in VMD. Each system contained approximately 110,000 atoms.

Each system was minimized for 10,000 steps, applying harmonic restraints of $20 \text{ kcal mol}^{-1} \text{ \AA}^{-2}$ to each atom in the graphene, and DNA if present. The systems were then equilibrated for 1.5 ns using a Nosé-Hoover Langevin piston, acting along the z direction only, to keep the pressure and temperature constant at 1 atm and 295 K, under the same restraints as those used during the minimization.

Production simulations under applied electric field were performed at constant volume, with the system’s dimensions set to the average values recorded during the equilibration simulations. Harmonic restraints of $10 \text{ kcal mol}^{-1} \text{ \AA}^{-2}$ were applied to the atoms of the graphene membrane restraining them to their initial coordinates. The electric field strength was set as $E = -V/L_Z$, where V was the target transmembrane bias and L_Z was the length of the simulation cell in the z direction.¹²

Simulations of DNA capture. In the simulations of the DNA capture, a custom tclforces script harmonically restrained the phosphorous atom of a DNA molecule to the surface of a cylinder (9.4 Å in radius) coaxial with the pore axis. The spring constant of each harmonic restraint was $1 \text{ kcal mol}^{-1} \text{ \AA}^{-2}$. These restraints allowed the DNA molecule to move toward and away from the graphene membrane, rotate freely about its axis, but remain coaxial with the pore axis. The same coaxial restraints were applied in the simulations of the stall

force, but additional restraints were used to maintain the distance between DNA and the graphene membrane. Specifically, the z coordinates of the DNA's phosphorous atoms were restrained to pre-determined initial values using harmonic potentials of $1 \text{ kcal mol}^{-1} \text{ \AA}^{-2}$ spring constants. The instantaneous stall force on DNA was obtained by averaging the instantaneous distance restraint forces over all phosphorous atoms and recorded every 200 fs.

To evaluate the rate of DNA capture, twenty simulation systems were created, each containing a DNA molecule placed initially coaxially with the pore and so that the center of mass of the closest base to the graphene membrane was 8 \AA away from the graphene membrane. Each simulation system was first equilibrated 1 ns with applied electric field and both coaxial and z -axis (DNA-graphene distance) restraints applied to the phosphorous atoms of DNA. After removing the z -axis restraints, the simulations were run until either the DNA completely translocated through the nanopore, or 20 ns had elapsed, whichever was shorter. The time elapsed from the removal of the distance restraints to the last time the center of mass of the leading DNA base crossed the plane of the graphene membrane was recorded as the capture time. The average capture rate was then calculated as the average of the inverse of the capture times. The DNA translocation time was calculated as the time from the moment the leading base of DNA crossed the plane of the graphene membrane for the last time until the trailing DNA base passed through the membrane plane.

Simulations of effective force. In the simulations of effective force on DNA, a custom `telforces` script harmonically restrained the phosphorous atom of a DNA molecule to the surface of a cylinder (9.4 \AA in radius) coaxial with the pore axis as in the simulations of DNA capture. The spring constant of each harmonic restraint was $1 \text{ kcal mol}^{-1} \text{ \AA}^{-2}$ except in simulations outlined in Supplementary Figure S7. These restraints allowed the DNA molecule to move toward and away from the graphene membrane, rotate freely about its axis, but remain coaxial with the pore axis. Additional restraints were used to maintain the distance between DNA and the graphene membrane. Specifically, the z coordinates of the

DNA's phosphorous atoms were restrained to pre-determined initial values using harmonic potentials of $1 \text{ kcal mol}^{-1} \text{ \AA}^{-2}$ spring constants. The instantaneous stall force on DNA was obtained by averaging the instantaneous distance restraint forces over all phosphorous atoms and recorded every 200 fs. To calculate the effective force, the distance restraint forces were averaged over several (3-5) 20 ns simulations.

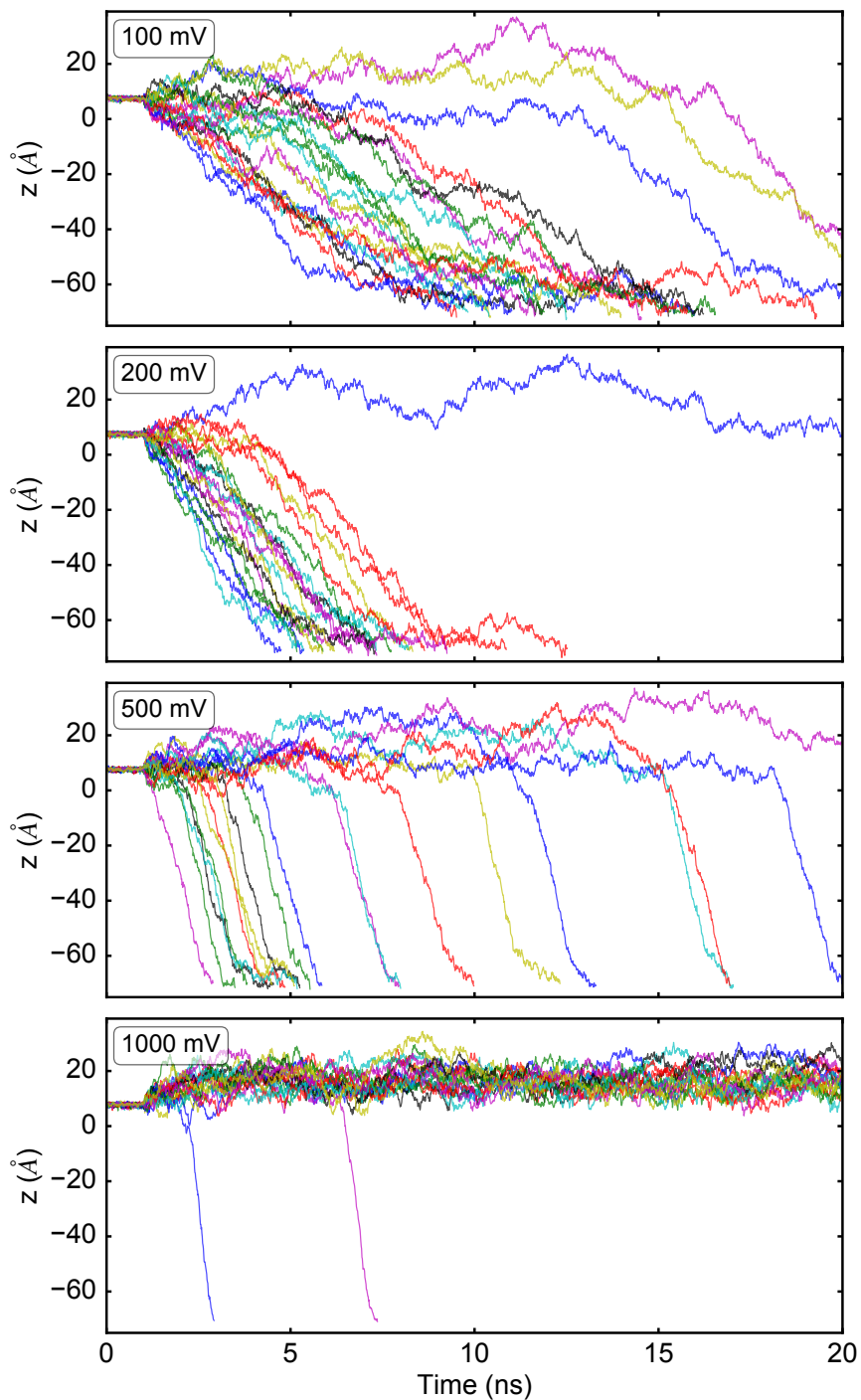
Simulation of hydrostatic compressibility. The hydrostatic compressibility of KCl solution was determined by simulating a cubic volume of solution (60 \AA on a side) in the NPT ensemble for at least 8 ns for pressure targets from 1 to 1000 atm. The simulations produced the dependence of the solution density on the solution pressure, Supplementary Figure S12, for 0 mM, 200 mM, 500 mM, 1 M, and 2 M KCl solutions. Because the ion concentration in the pore decreased at high transmembrane bias, the change in ion concentration was accounted for by measuring the density of ions and water separately and assigning a compressibility to each.

Local density of the water and ions was calculated by counting the number of water oxygen atoms and ions within a 1 nm radius cylinder coaxial with the pore. At each frame of an MD trajectory, atoms residing within this cylindrical volume were assigned to one of the 0.1 nm height bins; the local density values were obtained by averaging instantaneous density values over the simulation trajectories. The local pressure difference produced by a transmembrane bias was evaluated by measuring the local deviation of the solution density from the reference 0 V bias distribution and using the hydrostatic compressibility data from Supplementary Figure S12.

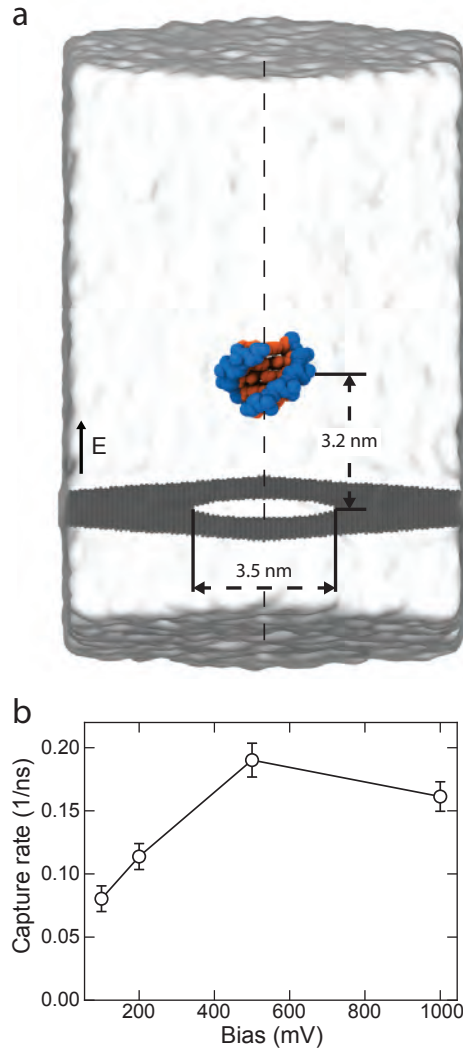
PMF calculations. PMFs were determined using the umbrella sampling method realized by means of the steered molecular dynamics (SMD) feature of NAMD. In each umbrella sampling simulation, the center of mass of the biomolecule was restrained to the nanopore axis, and to the specified distance from the graphene membrane, by using a harmonic restoring potential with a spring constant $k_s = 1600 \text{ pN/nm}$. The SMD velocity was set to zero in

each simulations. The sampling windows were spaced with a 2 Å interval along the nanopore axis. Each simulation was run for 30 ns; the first 5 ns of each MD trajectory were discarded before further analysis. The starting conformations for the umbrella sampling simulations were generated by a separate SMD run where a molecule was pulled along the nanopore axis with a constant velocity of 2 Å/ns for 16 ns. The PMFs were obtained using the WHAM protocol¹³ realized in the “WHAM: the weighted histogram analysis method” package, version 2.0.9.¹⁴

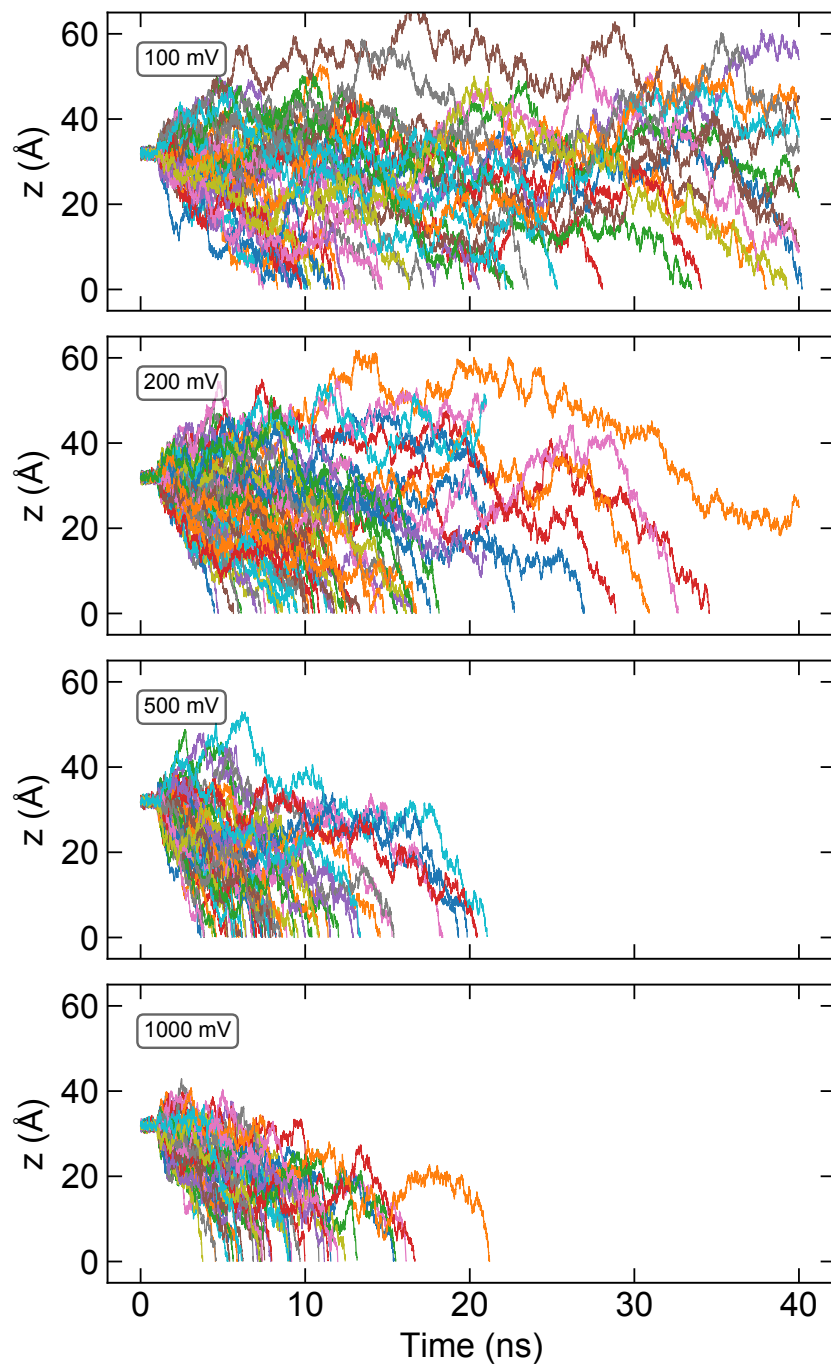
Electrostatic analysis. Maps of electrostatic potential were obtained using the PMEpot plugin¹⁵ of VMD, which stores the average (over trajectories) electrical potential in a 3D grid of ~ 1 Å spacing. A profile of the electrostatic potential along the nanopore axis, Supplementary Figure S14c, was then created by averaging the potentials over 1 nm radius disks arranged along the pore axis in 0.1 nm increments. Electric field (projected along the pore axis), Figure 3b and Supplementary Figure S9, was calculated by taking the derivative of the potential profile, and the derivative of the electric field was also calculated in order to calculate the dielectrophoretic force ($F_z = \mathbf{p} \cdot \hat{\mathbf{z}} \frac{\partial E_z}{\partial z}$) per water molecule, Figure 3d.



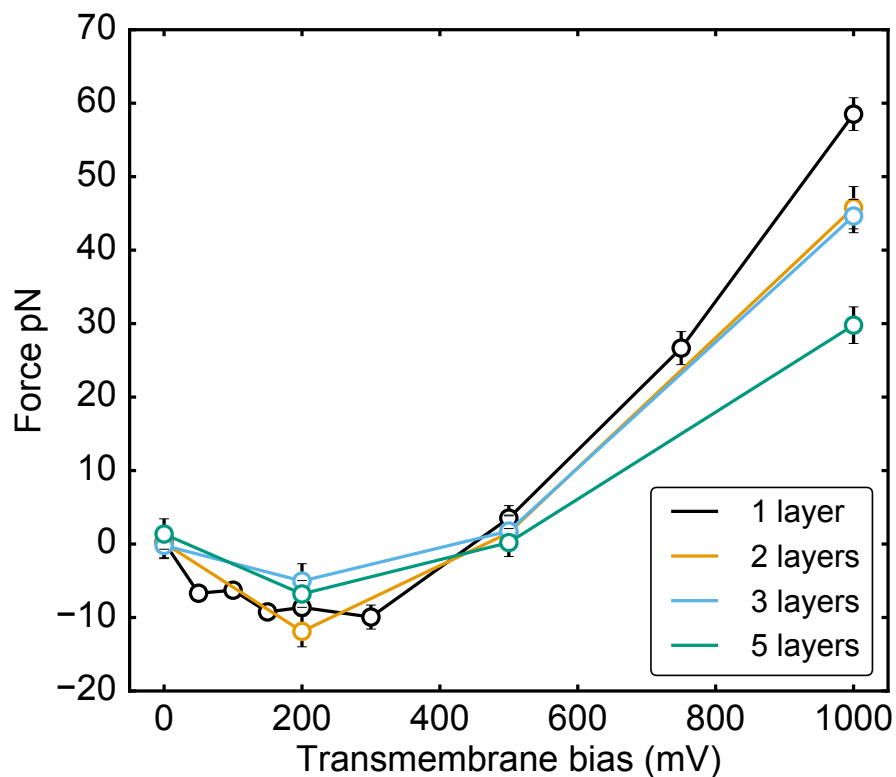
Supplementary Figure S1: MD simulations of DNA capture by graphene nanopore. For the first 1 ns of each simulation the DNA fragment was restrained and then released. Each panel shows the z -coordinate of the DNA's leading basepair versus simulation time for twenty independent simulations (each shown using unique color) carried out at the same transmembrane bias. The transmembrane bias magnitude is specified in each panel. The graphene membrane is located at $z = 0$. Our of twenty independent simulations, capture of DNA was not observed in zero, one, one and eighteen simulations carried out at 100, 200, 500 and 1000 mV, respectively.



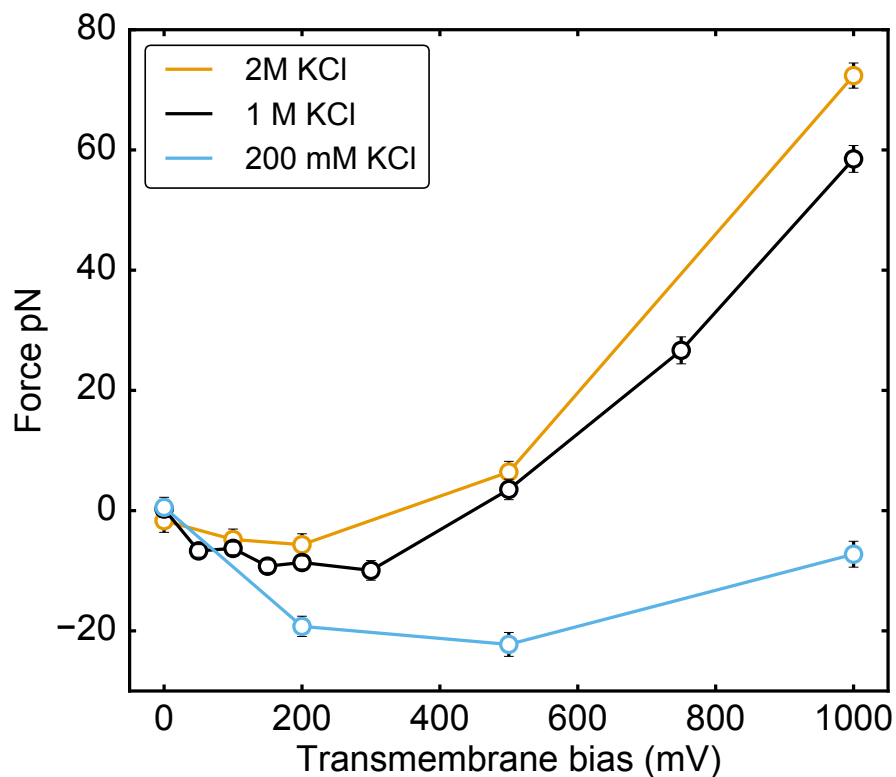
Supplementary Figure S2: Dependence of capture rate of a 5 bp dsDNA fragment on transmembrane bias. (a) A 5 bp dsDNA fragment was initially held so that its center of mass was located 3.2 nm from the midplane of the membrane along the nanopore axis. A transmembrane bias was then applied to the system. After 1 ns, the DNA was released. The fragment's center of mass was harmonically restrained to remain along the nanopore axis. (b) Capture rate of a 5 bp fragment of dsDNA versus transmembrane voltage. The time that it took from the release of the dsDNA until the moment the center of mass of dsDNA crossed the midplane of the pore was recorded. Forty independent simulations were performed at each transmembrane bias. The average of the inverse of the capture time, i.e. the average capture rate, is plotted in the figure. If the DNA was not captured within 40 ns, the DNA was assumed to be captured in 80 ns, which adds an error of at most 0.0125 ns^{-1} . Nine molecules were not captured at 100 mV, and one molecule was not captured at 200 mV within 40 ns. All were captured at 500 mV and 1 V. Traces from individual simulations are shown in Supplementary Figure S3.



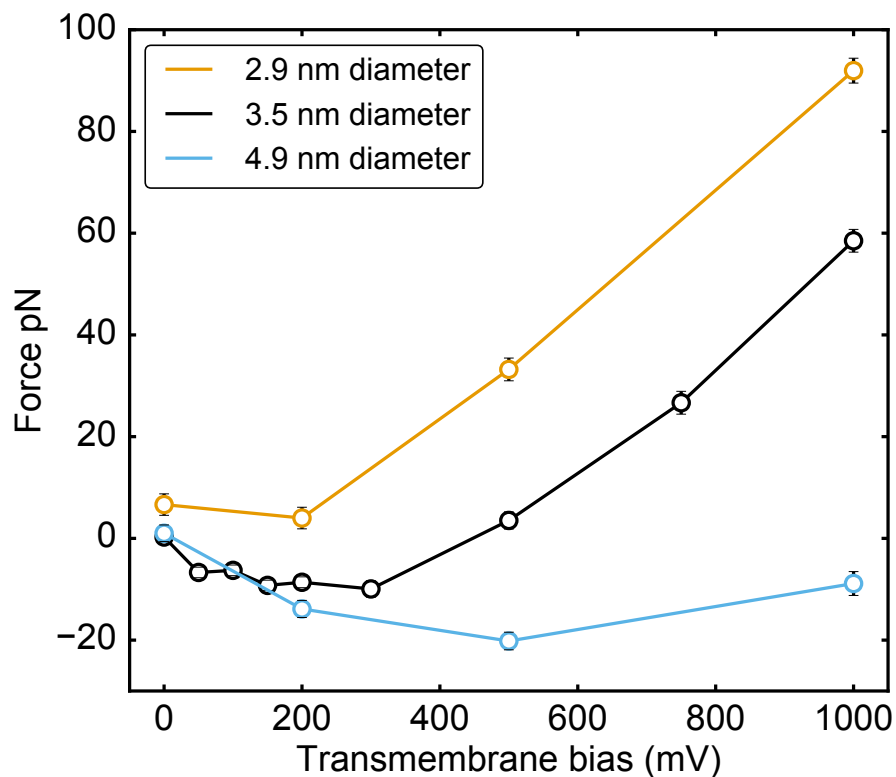
Supplementary Figure S3: The center of mass Z coordinate of the 5 bp dsDNA fragment during individual capture simulations. The average capture rate is plotted in Supplementary Figure S2



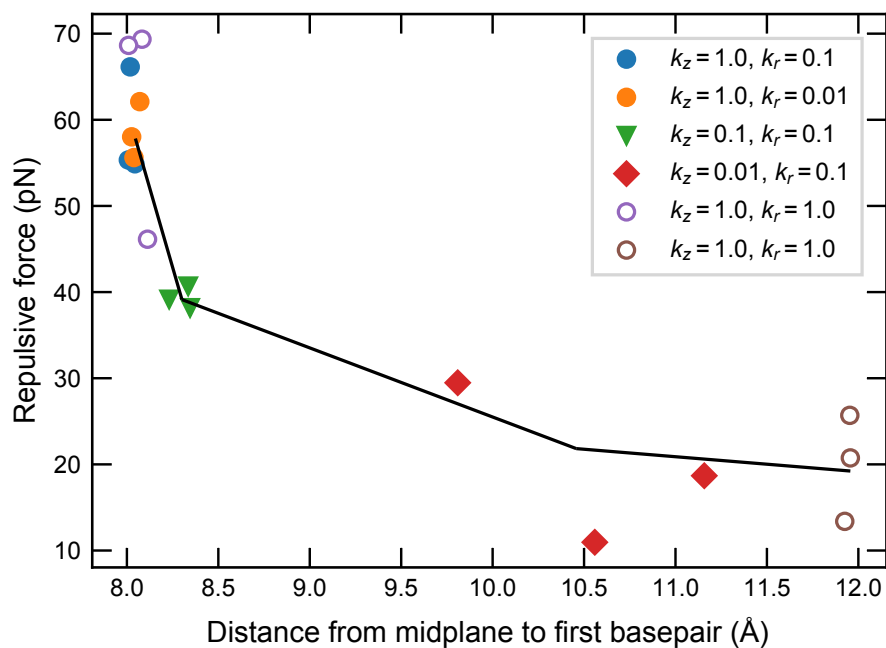
Supplementary Figure S4: Effect of membrane thickness on the effective force on DNA. In each simulation, the DNA molecule was restrained to remain coaxial with the nanopore and maintain the distance between the top layer of the graphene membrane and the nearest DNA base at 8 Å. All simulations were carried out in 1 M KCl solution; the nanopore diameter was 3.5 nm. Positive values of the effective force indicate repulsion of the DNA molecule from the nanopore. Lines are guides to the eyes.



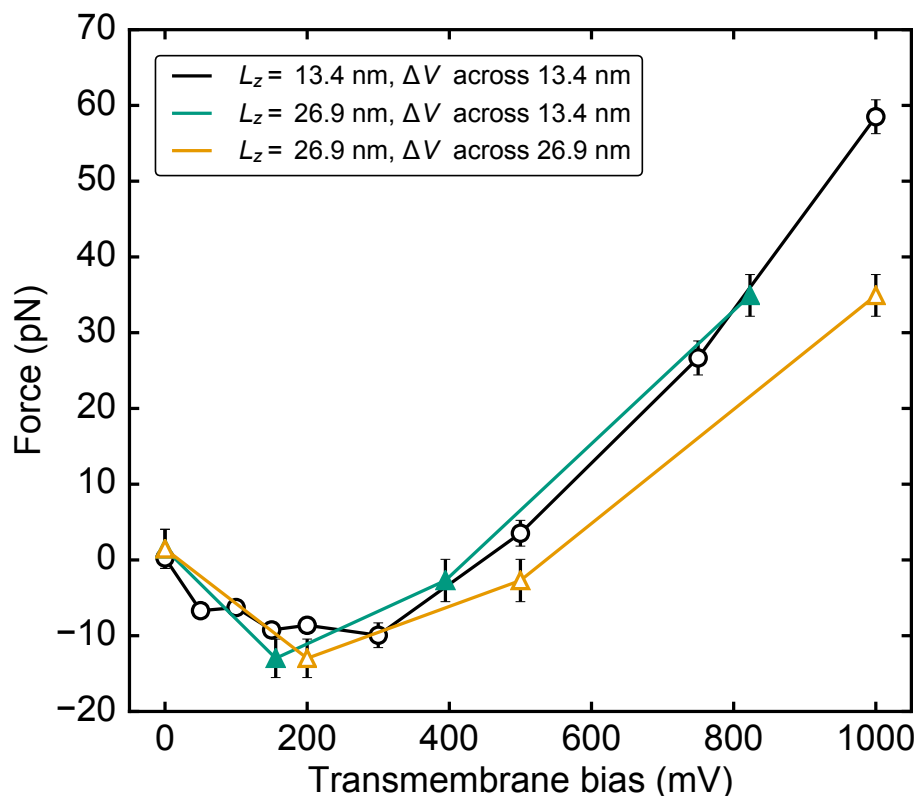
Supplementary Figure S5: Effect of ion concentration on the effective force on DNA. In each simulation, the DNA molecule was restrained to remain coaxial with the nanopore and maintain the distance between the top layer of the graphene membrane and the nearest DNA base at 8 Å. All simulations were carried out using a single-layer graphene membrane system; the nanopore diameter was 3.5 nm. Positive values of the effective force indicate repulsion of the DNA molecule from the nanopore. Lines are guides to the eyes.



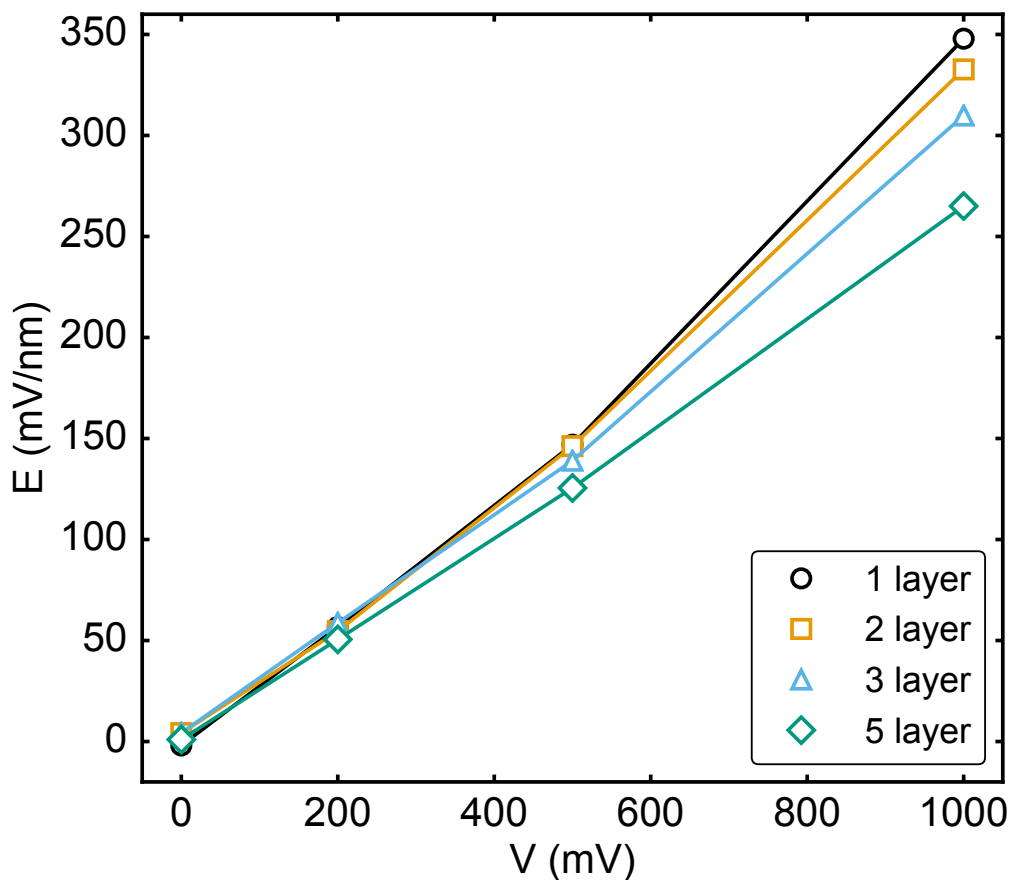
Supplementary Figure S6: Effect of pore diameter on the effective force on DNA. In each simulation, the DNA molecule was restrained to remain coaxial with the nanopore and maintain the distance between the top layer of the graphene membrane and the nearest DNA base at 8 Å. All simulations were carried out using 1 M KCl solution and single-layer graphene membrane. Positive values of the effective force indicate repulsion of the DNA molecule from the nanopore. Lines are guides to the eyes.



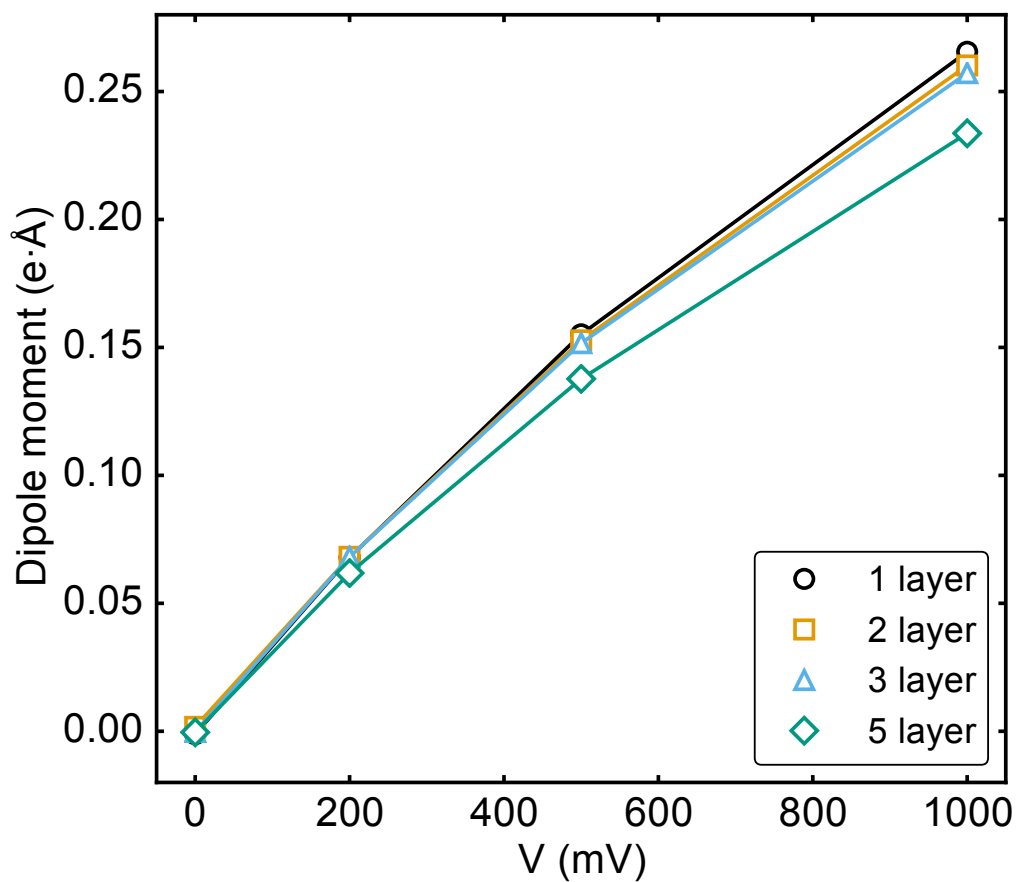
Supplementary Figure S7: Effect of restraint strength on the effective force on DNA. The phosphorous atoms of the DNA were restrained to remain on a cylinder coaxial with the nanopore of 9.4 Å radius with force constant k_r . They were also restrained to their initial z-coordinate with force constant k_z . The weak k_z restraints, $k_z = 0.1$ kcal/mol·Å² and $k_z = 0.01$ kcal/mol·Å² allow the DNA to move away from the pore and thus feel less repulsion force. Brown open circles represent simulations in which the first base pair of the DNA is held 12 Å from the midplane of the pore, all others represent simulations in which the first base pair of the DNA is held 8 Å from the midplane of the pore. Data displayed using open circles reproduces data from FIG 2b of the main text. All simulations were carried out using 1 M KCl solution and a single-layer graphene membrane. Three independent simulations were performed for each restraint strength. Positive values of the effective force indicate repulsion of the DNA molecule from the nanopore. Lines are guides to the eyes.



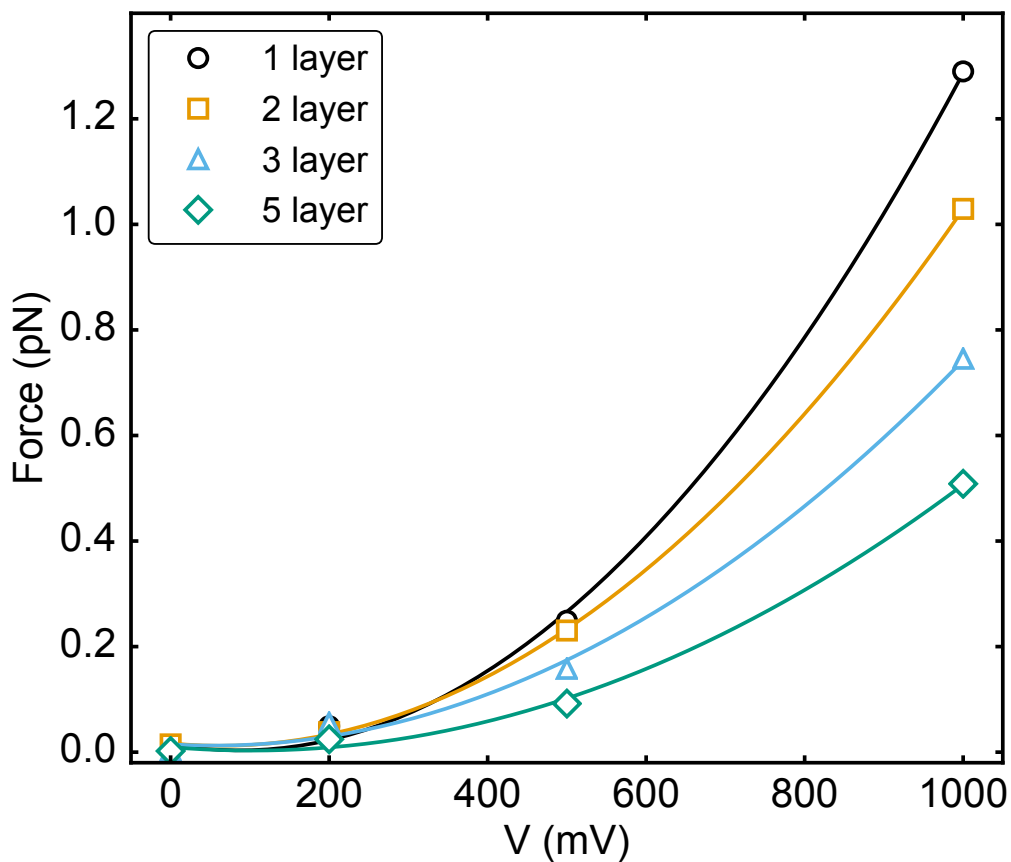
Supplementary Figure S8: Effect of simulation cell size on the effective force on DNA. In each simulation, the DNA molecule was restrained to remain coaxial with the nanopore and maintain the distance between the top layer of the graphene membrane and the nearest DNA base at 8 Å. The effective force on DNA is shown in open black circles (for simulation cell length 13.4 nm) and open orange triangles (for simulation cell length 26.9 nm). The effect of the extra access resistance incurred by using a longer simulation cell (see Supplementary Note 1 for further discussion) was removed by calculating the voltage drop across a 13.4 nm cell centered on the graphene, and plotting the force against this voltage (filled green triangles). Voltage was measured using the PMEpot plugin for VMD. All simulations were carried out using 1 M KCl solution and a single-layer graphene membrane. Positive values of the effective force indicate repulsion of the DNA molecule from the nanopore. Lines are guides to the eyes.



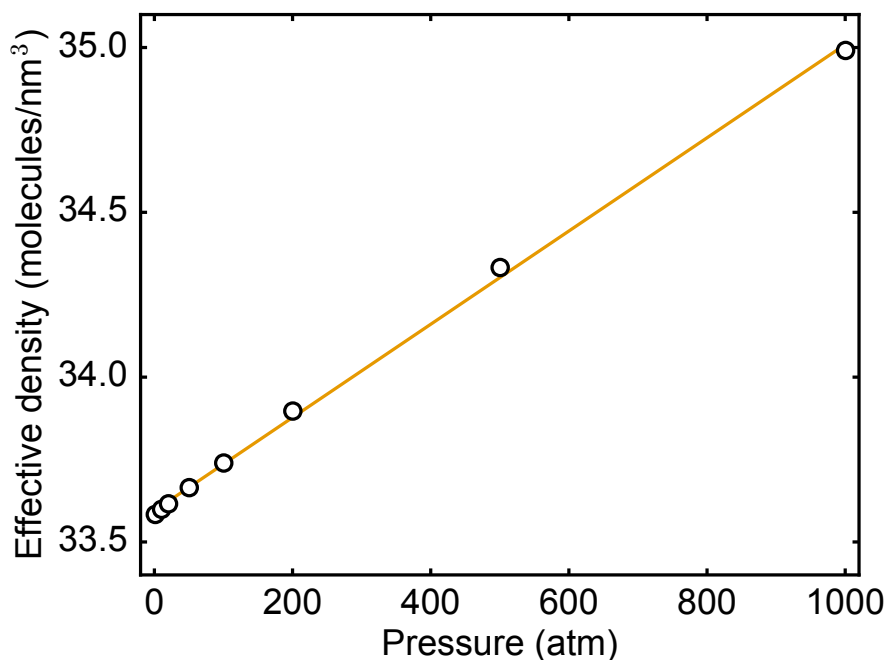
Supplementary Figure S9: Effect of transmembrane bias on the maximum electric field strength. The electric potential was measured using the PMEpot plugin for VMD, averaged over the respective MD trajectory. A 1D profile of the potential was created by averaging the potential values within 1 nm radius / 0.1 nm height cylindrical bins coaxial with the nanopore axis. The local electric field was determined as a gradient of the 1D potential. The data points shown in the graph were obtained by averaging the local electric field values over the bins centered within 0.5 nm of the graphene membrane midplane. Lines are guides to the eyes.



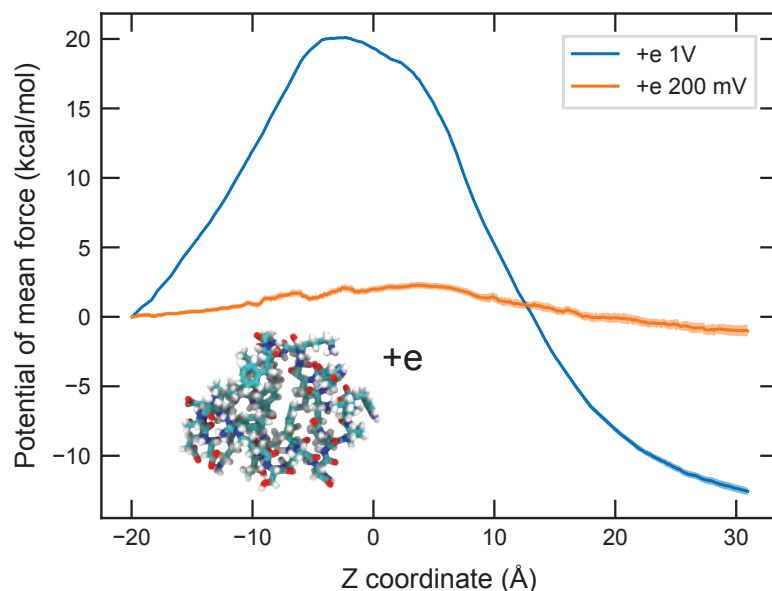
Supplementary Figure S10: Effect of transmembrane bias on the average z -component of a water molecule's dipole moment within a graphene nanopore. To compute the average values, instantaneous z components of water dipole moments were averaged over all water molecules residing within 1 nm-height / 1 nm-radius disk coaxial with the nanopore axis and centered at the nanopore center; the instantaneous values were then averaged over the respective MD trajectories. Lines are guides to the eyes.



Supplementary Figure S11: Effect of transmembrane bias on the maximum dielectrophoretic force on a water molecule. At each transmembrane bias, the dielectrophoretic force profile was calculated as described in the caption to main text Figure 3d. Here, we plot the maximum of the dielectrophoretic force profile against the transmembrane bias. Lines show quadratic fits to the data.



Supplementary Figure S12: Simulated dependence of solution density on solution pressure. The density of solution, $n = (N_w + k \cdot N_i)/V$, takes into account the relative volume that an ion takes up compared to a water molecule. In our simulations, at 1 M an ion takes up approximately 0.67 times the volume of a water molecule (N_w is the number of water molecules, N_i is the number of ions, V is volume, and $k = 0.67$ is the fraction of the volume of a water molecule that an ion takes on average). A linear fit to the dependence (orange line) has a slope of $0.00141 \text{ molecules/nm}^3 \cdot \text{atm}$, which is equivalent to a bulk modulus of $-2.41 \times 10^9 \text{ N/m}^2$ (using $\Delta n/n|_V \approx -\Delta V/V|_N$) at 1 atm. The experimental bulk modulus of pure water is $-2.17 \times 10^9 \text{ N/m}^2$.¹⁶ This constant establishes a correspondence between a surplus of atoms in a 1 nm^3 volume (over the atmospheric pressure value) and an increase in the local pressure. For example, increasing the local density by $1.41 \text{ molecules/nm}^3$ (about 4.2% change) corresponds to a 1000 atm increase in the local pressure.



Supplementary Figure S13: Potential of mean force of a villin headpiece protein along the symmetry axis of a 3.5 nm diameter nanopore under a 1 V (blue trace) or 200 mV (orange trace) transmembrane bias. This unmodified version of the villin headpiece protein has a charge of one proton. The graphene membrane is located at $Z = 0$. A successful capture of a protein corresponds to the Z coordinate change from negative to positive values. Note that the PMF plots displayed in this figure were computed using a smaller diameter nanopore than the PMFs reported in the main text Figure 4. A smaller nanopore exhibits a stronger water compression effect, which explains the presence of the translocation barrier at 200mV.

Supplementary Note 1: Effect of access resistance.

One difference between the model used in our all-atom MD simulations and the experimental setup is the location of the electrodes. In a nanopore experiment, the electrodes that produce a transmembrane voltage bias are located a macroscopic distance away from the nanopore – much too far to be explicitly modeled in an all-atom simulation. In our simulations, the effect of the electrodes is realized by the application of a constant electric field E_z throughout the simulation cell along the z axis, perpendicular to the membrane.^{12,15,17} This method, in effect, produces a non-uniform distribution of the electrostatic potential throughout the simulation domain with a constant potential difference $\Delta V = l_z \cdot E_z$ at the boundaries of the simulation cell. The boundaries of the simulation cell, separated by distance l_z , can be thought of as two electrodes having potentials V_1 and V_4 , see Supplementary Figure S14a.

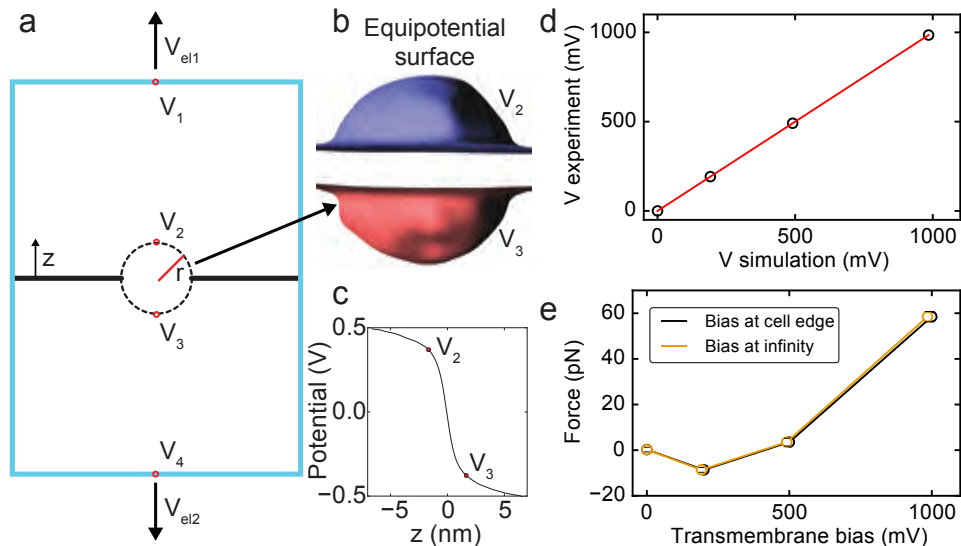
To compare the distributions of the electrostatic potential realized in experiment and simulation, we first analytically calculate the access, or spreading, resistance,¹⁸ the resistance from the pore mouth to the electrodes. Theoretically, the resistance of a volume confined between a hemisphere of radius r_p and a hemisphere that is infinitely far away is $R_a = \rho/2\pi r_p$, where ρ is the resistivity of the solution and r_p is the pore radius.¹⁸ In simulation, we can directly evaluate the potential at the hemisphere of radius r_p and combine the results with the above analytical model to evaluate experimental access resistance missing in the simulation. Here, we chose to use the hemisphere-to-hemisphere resistance model rather than the plate-to-hemisphere model¹⁹ because of the thinness of the graphene membrane.

Applying the PMEpot plugin of VMD¹⁵ to the 60 ns of MD trajectories of the open pore system (three independent simulations of 20 ns each) at each bias we evaluated the potential drop across the pore. A radially averaged potential profile was then obtained by averaging the 3D potential over 1 nm radius disks arranged along the pore axis in 0.1 nm increments, Supplementary Figure S14c. A linear interpolation to the resulting profile was used to find the potentials V_2 and V_3 at $z = \pm(r_p + t/2)$, where $t = 3.4 \text{ \AA}$ is the thickness of the graphene membrane. Supplementary Figure S14b shows the location of the V_2 and V_3 equipotential

hemispheres. Finally, the simulated pore resistance, R_p , was found by dividing the potential difference $V_2 - V_3$ by the ionic current passing through the pore: $R_p = (V_2 - V_3)/I$; the ionic current I was determined directly by the analysis of the MD simulations.

Now, we can relate the potential difference realized in our MD simulations $V_{\text{sim}} = V_4 - V_1$ to the equivalent experimental potential difference $V_{\text{exp}} = I(R_p + 2R_a)$, where I is the simulated ionic current, R_p is the pore resistance, $R_a = \rho/2\pi r_p$ and the factor of 2 accounts for access resistance of both *cis* and *trans* electrolyte compartments. Supplementary Figure S14d plots V_{sim} and V_{exp} against each other. The simulated and equivalent experimental transmembrane biases have very similar values for the periodic cell geometry chosen in our simulations. In general, the correspondence between the simulated and experimental bias conditions depends on the simulation cell geometry, for example, a longer and narrower simulation cell would have a higher resistance resulting in $V_{\text{sim}} > V_{\text{exp}}$.

Having established a mathematical relationship between the simulated and experimental transmembrane biases, we can now express the simulated values of the effective force on DNA as a function of the experimental voltage bias at infinity, Supplementary Figure S14e. For reference, we plot in the same figure the simulated dependence of the effective force on the transmembrane bias applied in the simulations (same as in main text Figure 2c). Because the access resistance terms effectively present in MD simulations and those that would be present in an equivalent experiment have similar values for the geometry considered in our simulations, both dependences follow one another closely.



Supplementary Figure S14: The effect of access resistance. (a) Schematic of the simulation system. V_1 and V_4 are the potentials at the "electrodes" (edge of the simulation cell) in the *cis* and *trans* compartments of the simulation system, respectively. V_2 is the potential at a distance r_p from the opening of the *cis* side of the pore, and V_3 is the potential at a distance r_p from the opening of the *trans* side of the pore. V_{el1} is the potential at an electrode in the *cis* chamber effectively infinitely far away, and V_{el2} is the corresponding electrode in the *trans* chamber. The access resistance of a nanopore is defined as the resistance of a volume confined between V_{el1} and V_2 and between V_3 and V_{el2} : $R_a = \rho/2\pi r_p$, where ρ is the resistivity of the solution, and r_p is the radius of the pore. (b) Equipotential surfaces at distance r_p from the nanopore opening obtained from the analysis of the MD trajectories. The blue and red surfaces indicate the hemisphere where the potential has values V_2 and V_3 , respectively. The values V_2 and V_3 were determined from the analysis illustrated in panel c. The 3D distribution of the electric potential was obtained by averaging instantaneous potential distributions realized in three independent 20 ns simulations of the open pore system at a 1 V transmembrane bias. (c) Radially averaged electric potential along the nanopore axis obtained by averaging the 3D potential (panel b) over 1 nm radius disks arranged along the pore axis in 0.1 nm increments. Potential at a distance r_p from either nanopore opening, V_2 and V_3 , are shown by filled red circles. The pore resistance (between V_2 and V_3) is given by $R_p = (V_3 - V_2)/I$. (d) Potential difference at infinity (using the formula for access resistance) that would cause the same transmembrane bias as in simulation versus potential difference across the simulation cell. (e) Simulated effective force on DNA versus transmembrane bias applied in the simulations $V_s = V_1 - V_4$ (black circles) and versus equivalent experimental bias at infinity, $V_{inf} = V_{el1} - V_{el2}$ computed as $V_{inf} = I(R_p + 2R_a)$.

Supplementary Note 2: Continuum model of the nanopore pressure.

To obtain an independent evaluation of the pressure inside the nanopore volume, we obtained the distribution of the electric field in the vicinity of the graphene nanopore systems through finite element calculations carried out with the COMSOL software package (COMSOL Multiphysics 4.3). The system consisted of a cylindrically symmetric space of height $L_z = 12$ nm, and radius $R = 6$ nm, Supplementary Figure S15a, a membrane of thickness $t = 0.3$ nm, and a nanopore of radius $r_p = 1.75$ nm cut out of the membrane, matching the dimensions of the MD system.

The distribution of the electric potential was calculated by solving coupled electrostatics and ion diffusion equations using the electrostatics and transport of dilute species modules, respectively. The upper and lower boundaries of the system were set to have the prescribed positive bias (+200, +500, or +1000 mV) and 0 V, respectively; the concentration of KCl solution was set to 1 M. The graphene surface and the outer radius of the cylindrical system had "zero charge" and "no flux" conditions applied. Supplementary Figure S15b shows the electric potential profile along the pore axis for several transmembrane biases.

The force on each water molecule due to its dipole moment was calculated as

$$F_d = (\mathbf{p} \cdot \nabla)\mathbf{E}$$

where \mathbf{p} was the dipole moment of a water molecule, and \mathbf{E} was the electric field. Considering only the force component along the nanopore axis (or z axis),

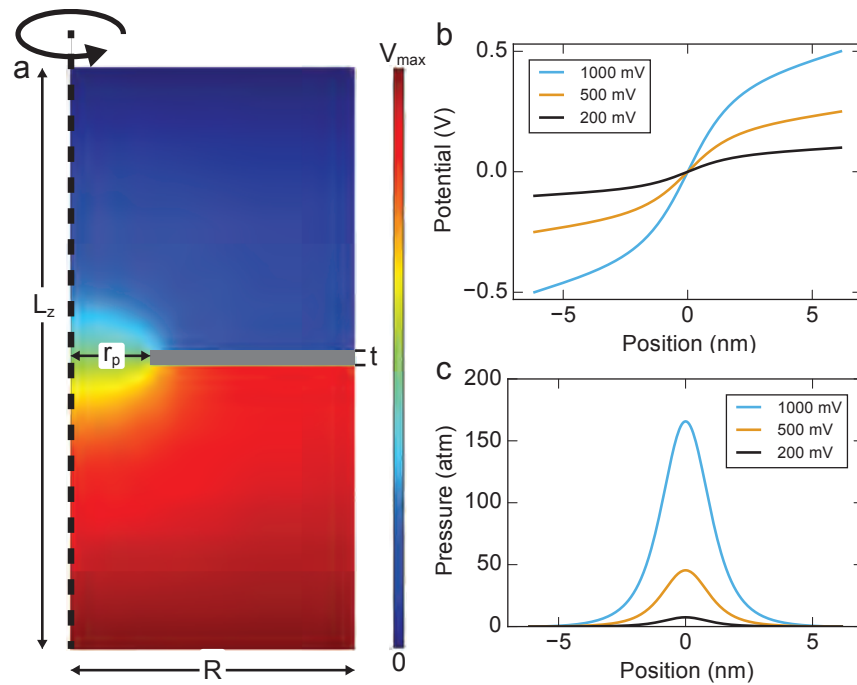
$$F_d = p_z \frac{\partial E}{\partial z}$$

where p_z is the projection along the nanopore axis of the dipole moment of a water molecule.

Booth formula^{20,21} was used to evaluate polarization of water in electric field:

$$p_z(E_z) = \frac{(n^2 - 1)}{4\pi} E + \frac{\alpha(n^2 + 2)\mu}{4} L\left(\frac{\beta(n^2 + 2)\mu E}{kT}\right)$$

where $\alpha = \frac{28}{3\sqrt{73}}$, $\beta = \frac{\sqrt{73}}{6}$, $n = 1.33$ is the index of refraction of water, T is the temperature, k is the Boltzmann constant, $\mu = 0.489$ eÅ is the dipole moment of water, and $L(x) = \coth x - \frac{1}{x}$ is the Langevin function. Integrating F_d from the system's boundary along the nanopore axis gives an estimate of the local water pressure. The local pressure obtained in this way is plotted along the nanopore axis for several values of the transmembrane bias in Supplementary Figure S15c.



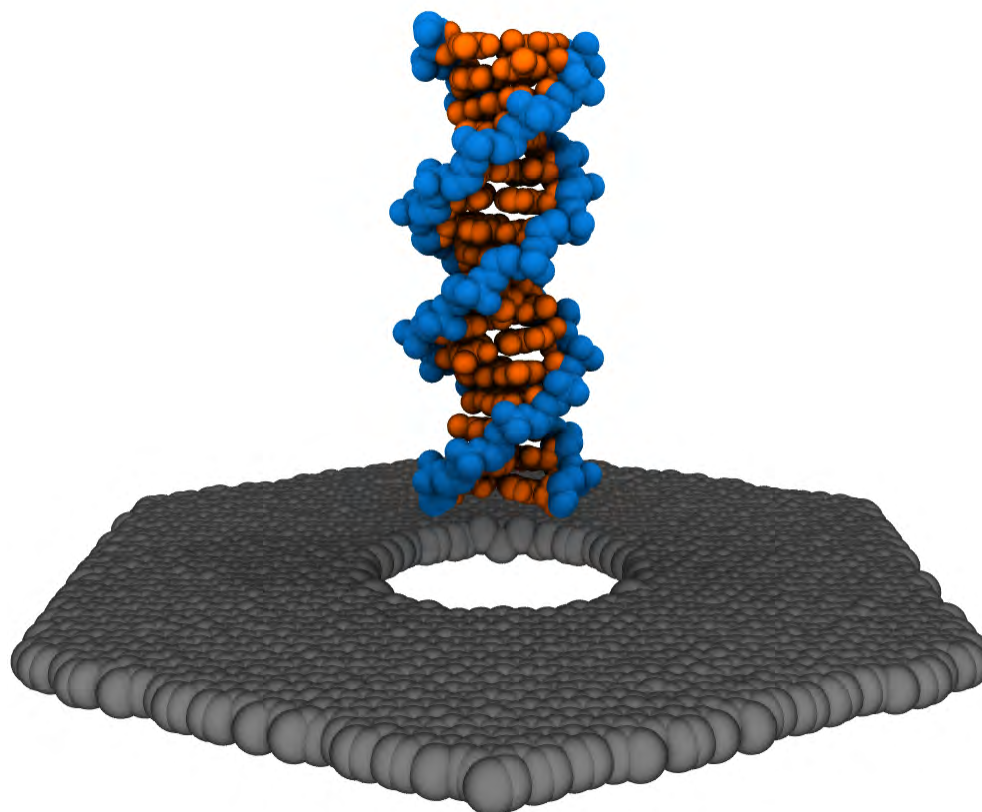
Supplementary Figure S15: Finite element model of the nanopore system. (a) Cylindrically symmetric nanopore system of height $L_z = 12$ nm and radius $R = 6$ nm. The graphene has thickness $t = 0.3$ nm. (b) The electrical potential along the nanopore axis resulting from continuum calculations. (c) Local hydrostatic pressure along the nanopore axis calculated from the electrostatic potential.



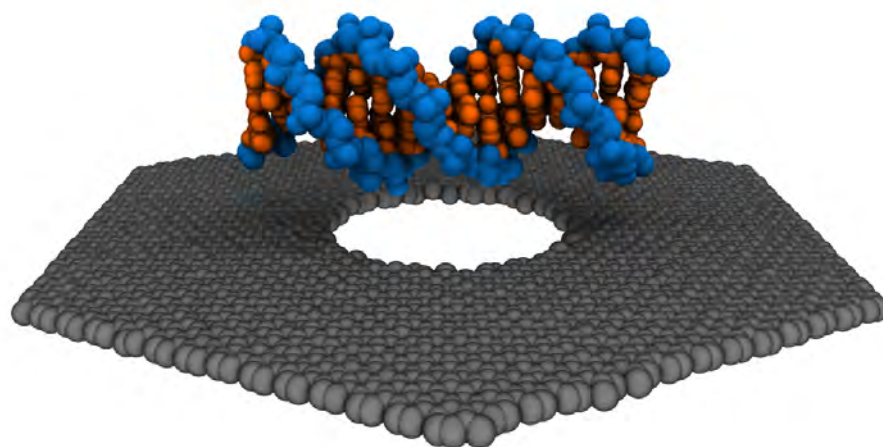
Supplementary Movie 1: Animation illustrating a 10 ns MD trajectory of a dsDNA molecule translocating through a nanopore in a graphene membrane under a 100 mV bias. Harmonic restraints were applied to the DNA molecule to maintain its coaxial arrangement with the nanopore. Graphene atoms are shown as gray spheres. Some graphene atoms are not shown to depict the location of the pore more clearly.



Supplementary Movie 2: Animation illustrating a 20 ns MD trajectory of a dsDNA molecule failing to translocate through a graphene membrane under a 1 V bias. Harmonic restraints were applied to the DNA molecule to maintain its coaxial arrangement with the nanopore. Graphene atoms are shown as gray spheres. Some graphene atoms are not shown to depict the location of the pore more clearly.



Supplementary Movie 3: Animation illustrating a 20 ns MD trajectory of a dsDNA molecule held above a graphene membrane under a 1 V bias. Harmonic restraints were applied to the DNA molecule to maintain its coaxial arrangement with the nanopore. Graphene atoms are shown as gray spheres. DNA is able to rotate about its helical axis.



Supplementary Movie 4: Animation illustrating a 20 ns MD trajectory of a dsDNA molecule held above a graphene membrane parallel to the membrane under a 1 V bias. Harmonic restraints were applied to the DNA molecule to maintain its parallel arrangement with the nanopore. The DNA is able to rotate about its helical axis and about the pore axis. Graphene atoms are shown as gray spheres.

Supplementary References

- (1) Phillips, J. C.; Braun, R.; Wang, W.; Gumbart, J.; Tajkhorshid, E.; Villa, E.; Chipot, C.; Skeel, R. D.; Kale, L.; Schulten, K. *J. Comput. Chem.* **2005**, *26*, 1781–1802.
- (2) MacKerell, Jr., A. D. et al. *J. Phys. Chem. B* **1998**, *102*, 3586–3616.
- (3) Wells, D. B.; Belkin, M.; Comer, J.; Aksimentiev, A. *Nano Lett.* **2012**, *12*, 4117–4123.
- (4) Yoo, J.; Aksimentiev, A. *J. Phys. Chem. Lett.* **2012**, *3*, 45–50.
- (5) Miyamoto, S.; Kollman, P. A. *J. Comput. Chem.* **1992**, *13*, 952–962.
- (6) Andersen, H. C. *J. Comput. Phys.* **1983**, *52*, 24–34.
- (7) Darden, T. A.; York, D.; Pedersen, L. *J. Chem. Phys.* **1993**, *98*, 10089–92.
- (8) Koopman, E. A.; Lowe, C. P. *J. Chem. Phys.* **2006**, *124*, 204103.
- (9) Humphrey, W.; Dalke, A.; Schulten, K. *J. Mol. Graphics* **1996**, *14*, 33–38.
- (10) Aksimentiev, A.; Brunner, R.; Cruz-Chu, E. R.; Comer, J.; Schulten, K. *IEEE Nanotechnol. Mag.* **2009**, *3*, 20–28.
- (11) van Dijk, M.; Bonvin, A. M. J. J. *Nucleic Acids Res.* **2009**, *37*, W235–W239.
- (12) Aksimentiev, A.; Heng, J. B.; Timp, G.; Schulten, K. *Biophys. J.* **2004**, *87*, 2086–2097.
- (13) Kumar, S.; Rosenberg, J. M.; Bouzida, D.; Swendsen, R. H.; Kollman, P. A. *J. Comput. Chem.* **1992**, *13*, 1011–1021.
- (14) Grossfield, A.
- (15) Aksimentiev, A.; Schulten, K. *Biophys. J.* **2005**, *88*, 3745–3761.
- (16) Rodnikova, M. *J. Mol. Liq.* **2007**, *136*, 211–213.

- (17) Roux, B. *Biophys. J.* **2008**, *95*, 4205–4216.
- (18) Hille, B. *Prog. Biophys. Mol. Biol.* **1970**, *21*, 1–32.
- (19) Hall, J. E. *J. Gen. Physiol.* **1975**, *66*, 531–532.
- (20) Gutiérrez, S. A.; Bodrenko, I.; Scorciapino, M. A.; Ceccarelli, M. *Phys. Chem. Chem. Phys.* **2016**, *18*, 8855–8864.
- (21) Booth, F. *J. Chem. Phys.* **1951**, *19*, 391–394.